I&EC research
Industrial & Engineering Chemistry Research

Article

pubs.acs.org/IECR

Optimal Design of a Corrugated-Wall Photocatalytic Reactor Using Efficiencies in Series and Computational Fluid Dynamics (CFD) Modeling

Claudio Passalía, Orlando M. Alfano, and Rodolfo J. Brandi*

FICH—Departamento de Medio Ambiente, Facultad de Ingeniería y Ciencias Hídricas, Universidad Nacional del Litoral, Ciudad Universitaria, (3000) Santa Fe, Argentina

INTEC—Instituto de Desarrollo Tecnológico para la Industria Química (CONICET−UNL) Güemes, 3450 (3000) Santa Fe, Argentina

ABSTRACT: The optimization of a corrugated wall photocatalytic reactor for air treatment was addressed using the concept of efficiencies in series. A new concept has been introduced: the inner incidence efficiency, associated with the internal configuration of the reactor (for instance, the folding angle in the considered case). The goal of the study was to obtain an optimum for the folding angle, subjected to certain constraints: fixed reactor volume, radiation flux, and gas flow rate. Previous experimentally determined degradation kinetics of a gaseous pollutant was used in the reactor modeling. The simulations of the reactor were performed computationally by using a computational fluid dynamics (CFD) package. The results showed opposed behaviors for the relative catalytic area per unit window area and the relative incident flux with the folding angle. Given that the inner incidence efficiency comprises the product of the two mentioned variables, an optimal folding angle was identified.

1. INTRODUCTION

General concern about indoor air quality problems has risen in the last few decades. Given that people spend most of their time in confined environments, indoor air quality and pollution are considered key aspects regarding human health.[1−3]

Indoor air quality may be controlled by heterogeneous photocatalysis, which is an effective alternative to conventional technologies that has been probed to chemically destroy a large variety of airborne pollutants. In a photocatalytic reactor, the compounds contained in the air stream may be adsorbed onto the surface of the irradiated catalyst, where a series of superficial reactions can, ultimately, eliminate the pollutants. Generally, the organic pollutants are converted into harmless, simple inorganic compounds, such as water and carbon dioxide.

Photocatalytic wall reactors must provide the contact among three entities at once: the molecules of reactant, the surface where the photocatalyst particles are immobilized, and the radiation energy at the proper wavelength. Thus, the modeling of such reactors presents an additional complexity: the need for solving the radiation field in addition to the classical momentum, energy, and species mass balances.

The design fundamentals of photocatalytic reactors are based on the classic chemical engineering balances, with the addition of the radiative transfer equation.[4,5] Photocatalytic reactors used for gas-phase purification have a relatively small number of possible configurations which are very different to each other. However, all of the designs must include an immobilization of the catalyst to some support material. Among the geometries or configurations of photocatalytic wall reactors that have been studied and present satisfactory efficiencies, one may mention the following: the monolith and honeycomb reactors,[5] the mesh reactor,[6] the annular or multiannular reactor,[7] the flat plate reactor,[8,9] the multiplate reactor,[10] and the corrugated reactor.[11,12]

In order to perform trustable comparisons among different reactor configurations and their performances, a comparison criterion must be defined. Such a performance parameter for photocatalytic reactors must be independent of the operating conditions, reactor geometry, and catalyst nature. In this regard, some authors have developed valuable concepts such as the quantum yields,[7,13] the photonic efficiencies,[14,15] and the electrical energy per order or per unit mass.[16] A different parameter was also proposed: the photochemical thermodynamic efficiency factor.[17] Similarly, a novel insight was developed introducing the concept of mass-transfer units.[18]

The present work is aimed at the definition and application of photoreactor efficiencies to provide design criteria for the optimization of such devices. To this aim, the concept of multiple independent efficiencies in series contributing to the overall reactor performance is applied. This approach, based on the works by Cerdá et al.[19] and Imoberdorf et al.,[7] is extended and applied here; it allows the identification of reactor design advantages and drawbacks, offering useful tools for subsequent optimization.

Having established the comparison criteria and design parameters, the individual efficiencies are then applied and computed for a corrugated wall reactor in order to identify a possible optimum folding angle. A previous experimentally determined degradation kinetics for formaldehyde in air[9] is used in the computational simulations. The entering radiation flux is evaluated through a ray-tracing-based algorithm written ad hoc; the radiation interchange inside the reactor is modeled through the use of local view factors. Finally, the mass balance

Received: October 16, 2012
Revised: March 7, 2013
Accepted: April 25, 2013
Published: April 25, 2013

dx.doi.org/10.1021/ie302838m | *Ind. Eng. Chem. Res.* 2013, 52, 6916−6922

for the pollutant in the reactor is solved using a CFD package in which the radiation boundary conditions, reflection and absorption phenomena, as well as the degradation kinetics, are introduced by custom-defined functions. The influence of the fraction of reflected radiation on the incidence efficiency is also studied.

2. FUNDAMENTALS

2.1. Photoreactor Design Features. Given a certain polluted air stream with known flow rate and pollutant concentration to be treated, photocatalytic reactors require a careful design and the selection of several parameters,[4] including (i) the UV radiation source; (ii) the geometrical arrangement of the radiation source, with respect to the reaction space; (iii) the type of fluid dynamic operation (continuous flow, batch, semibatch, recycle, etc.); (iv) the inner reactor geometry (shape and dimensions); and (v) the photocatalyst nature (which includes optical and catalytic properties, stability, deactivation, and the interaction among radiation, the catalyst, and the fluid).

When treating polluted air streams, it is required that the TiO_2 be fixed on some material acting as a support, since the catalyst should not be dragged by the gas stream. The two types of catalyst immobilization on the support material are (i) dispersion in a matrix that serves as support and (ii) as photocatalyst coatings, layers, or films. The purpose is to obtain the largest possible surface area exposed to radiation and good adhesion to an inert substrate.

Given a certain irradiation system, the possibilities of exposing a reactor volume to it are many. The key aspect regarding the outer configuration is how the reactor "window"—the area of radiation entrance to the reactor—is exposed to the radiation source. This outer configuration is independent of the way the reactor makes profit of the radiation within its inner volume. In order to compare these configurations, one might consider a global outer configuration efficiency.

The outer configuration efficiency may be thought as a global configuration factor, such as the usually defined in the radiation transfer bibliography.[20,21] The view factors are integrated forms which have been tabulated for many different geometries. One of the simplest is the flat plate reactor; other configurations include the annular reactor, the corrugated reactor, and the monolith reactor. Of course, these geometries have advantages and drawbacks, depending on the application needed.

2.2. Definition of Efficiencies. An analysis of the factors affecting the photoreactor performance may be carried out by considering the overall behavior as a series of interlinked phenomena; the individual processes have a unique probability of occurrence or efficiency, which may be estimated.

The total quantum efficiency (η_T), defined as the ratio of pollutant molecules decomposed to photons emitted by the radiation source, can be used to determine the reactor performance and compare different operating conditions or reactor configurations; yet, it is interesting to discriminate in which way a series of successive events, each one having its own efficiency, determine the final η_T value.[19]

In the first term, the radiation source has a certain capacity of converting electrical energy (actually consumed power, P) into emitted radiant power (P_L) with a given *electrical efficiency*:[19] $\eta_{ele} = P_L/P$. This parameter has a fixed value for a given brand and model of lamp. Nevertheless, in the computation of η_{ele}. it is relevant the definition of the spectral output power limits, since the lamp may emit radiation at wavelengths that cannot be used by the catalyst; in this way, one may account for all of the electrical energy transformed into radiant energy of any wavelength or limit this integration to the range in which the catalyst absorbs radiation.

Once the photons of the desired wavelength are emitted by the lamp, they may or may not reach the reactor entering surface(s) (windows). The possibility of occurrence of such event may be called η_{inc}^{out}, the *outer geometrical incidence efficiency*, and is defined by

$$\eta_{inc}^{out} = \frac{\int_{A_W}\int_{\lambda} q_{\lambda,W}^{out}\, d\lambda\, dA}{\int_{\lambda} P_{\lambda,L}\, d\lambda} = \frac{\langle q_W^{out}\rangle A_W}{P_L} \quad (1)$$

The outer geometrical or configurational efficiency, as presented in eq 1, is the ratio between the radiative energy that reaches the reactor window and the output power of the lamp in the useful wavelength range. It is a relative optical parameter between the radiation source and the surface of entering radiation to the reactor. The reactor geometry and the lamp arrangement to irradiate the reactor are the solely parameters determining this efficiency. The definition of the denominator in eq 1 must take into account the number of lamps and the presence of reflectors.

A fraction of the photons that get to the reactor window is transmitted; once inside, they can either reach or not a catalytic surface. In this way, the *inner incidence efficiency*, which is defined as

$$\eta_{inc}^{in} = \frac{\langle q_{inc}\rangle A_{cat}}{\langle q_W\rangle A_W} \quad (2)$$

can be interpreted as the probability of a radiation ray leaving the inner side of the reactor window to get to a catalytic area. The numerator in eq 2 represents the amount of incident energy that can activate the photocatalyst, whereas the denominator is the amount of energy entering the reactor. Note that the average radiation flux in the reactor window takes into account the attenuation due to the window material transmittance, by the relation: $\langle q_W\rangle = \tau\langle q_W^{out}\rangle$. The incident radiation flux, $\langle q_{inc}\rangle$, is averaged over the catalyst surface area; on the other hand, $\langle q_W^{out}\rangle$ is also area-averaged, but with respect to the reactor window area.

The inner incidence efficiency represents a new contribution of the present work that emerges as a key parameter regarding photoreactor design. Notice that the internal configuration of the reactor may allow the enhancement of this efficiency by surface-to-surface radiative interaction through reflection. Here, the optical properties of the support material are very important, because transmittance or reflection may have a positive or negative impact, depending on the shape and configuration of the reactor. For instance, in a multiannular reactor, a material with the largest transmittance is preferred, whereas in a corrugated wall an opaque support and catalyst reflection may be useful.

It is worth noting that an "incidence efficiency" has been used in the past,[7,19] which may be thought as the product of the inner and outer geometrical efficiencies here described. Although it may be useful in some cases, the incidence efficiency may be insufficient, given that it combines two very different aspects of the reactor configuration. The splitting of this parameter into outer and inner effects allows to identify

dx.doi.org/10.1021/ie302838m | Ind. Eng. Chem. Res. 2013, 52, 6916−6922

which one has the largest impact on the overall reactor performance.

Eventually, the radiation that reaches the catalyst surface may be absorbed or reflected, giving place to another parameter, η_{abs}, which is the *absorption efficiency*:

$$\eta_{abs} = \frac{\langle e^{a,s}\rangle A_{cat}}{\langle q_{inc}\rangle A_{cat}} \tag{3}$$

where $e^{a,s}$ is the local superficial rate of photon absorption (LSRPA),[4] with units of moles of photons per unit area and time. Equation 3 is simply the ratio between absorbed and incident energy on the catalytic surface. It is independent of the external reactor geometry, but an intrinsic property of the photocatalyst nature; in determinations of the optical parameters, this efficiency may be thought as the absorbed fraction of incident radiation.

Finally, the reaction efficiency is defined as

$$\eta_{rxn} = \frac{\langle R_{sup}\rangle A_{cat}}{\langle e^{a,s}\rangle A_{cat}} \tag{4}$$

The reaction efficiency can be regarded as the number of pollutant units (moles) eliminated per absorbed energy (moles of photons or einsteins) over the catalyst surface.

The global efficiency (η_T) is defined as the product of individual efficiencies, according to

$$\eta_T = \prod_i \eta_i = \eta_{ele}\eta_{inc}^{out}\eta_{inc}^{in}\eta_{abs}\eta_{rxn} \tag{5}$$

In this sense, it is worth noting some issues regarding how these efficiencies are coupled. Neither the electrical efficiencies nor the following defined efficiencies are strictly independent. The efficiencies are linked by the optical properties of the lamps (output spectral power), the transmittance of the window material and the spectral absorption of the layer of immobilized catalyst. In fact, the range of wavelengths in which the integration of properties is performed determines the coupling among the different efficiencies. In addition, it can be seen in eq 5 that the product of the inner and outer incidence efficiencies reconstructs the incidence efficiency presented in the literature.[7,19]

3. APPLICATION: CORRUGATED WALL PHOTOCATALYTIC REACTOR

Corrugated wall reactors offer the advantage of presenting a large catalytic area per unit volume. Besides, as previously noted, the configuration allows the radiative interaction between walls, which may result in an additional gain in the use of radiation. Among the possible corrugated geometries, the most simple is the one with triangle-shaped channels. It is a geometry that has been previously studied and experimentally applied.[11,12]

In a previous work, a corrugated wall photoreactor was studied and modeled.[12] The reactor consisted of an acrylic box irradiated by two sets of actinic UV lamps with a folded plate inside forming a set of triangular section channels, as seen in Figure 1. The corrugated plate was made of stainless steel and coated with titanium dioxide by means of an impregnation technique. The reactor operates in a continuous mode, with one pass. The air stream inside the reactor follows a zigzag pattern alternating the direction of flow from one channel to

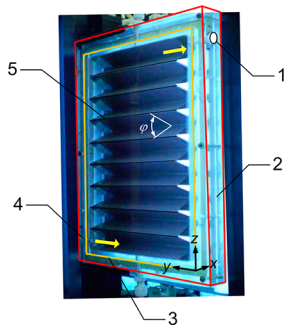

Figure 1. Corrugated wall reactor scheme. Legend: (1) reactor outlet, (2) acrylic frame, (3) reactor window, (4) reactor inlet, and (5) TiO_2-coated stainless steel.

the following. The folding angle and the coordinate system are also schematically depicted in Figure 1.

3.1. Comparison Criteria. In order to apply the proposed efficiencies, the question of fixed parameters arises. The choice between the possible geometrical or operational variables to be kept fixed determines largely the possibilities for comparing different reactor configurations.

On the one hand, a practical problem needing solution would present a given gas flow rate (Q_g) and a pollutant concentration ($C_{i,0}$) to be reduced. These operational variables are indeed kept constant throughout the evaluation of efficiencies for different reactor configurations. Also, the radiation source (or, equivalently, the radiation flux reaching the reactor windows) could be considered fixed, given that the goal is to find the best reactor configuration. On the other hand, some other variables should be kept constant to allow the comparison. In this sense, an engineering approach has been used: the reactor volume and the area of radiation entrance to the reactor (window areas) were kept fixed. This criterion also takes into account the restrictions of available space for the reactor and the radiation source.

When the aforementioned restrictions are applied to a corrugated wall reactor attempting to detect an optimal configuration, the folding angle remains as the only adjustable parameter. The direct effect of modifying the folding angle is that the size and number of channels must change. The latter is increased with the reduction in the folding angle, while the size of each channel is consequently reduced to maintain the total reactor volume constant.

A study was performed by simulation of the reactor performance for different folding angles (φ). The upper limiting case for a given volume and reactor window is, of course, the flat plate reactor, $\varphi = 180°$. The other folding angles modeled were 97.2°, 59.1°, 31.6°, and 15.2°. With these angles, the number of triangular section channels rises from 2 to 4, 8, and 17, respectively. In all cases, the total reactor volume was kept at 365 cm^3. The useful length of the channels is 16 cm, i.e., the length where the catalyst is immobilized.

3.2. Reactor Modeling. The reactor configurations were all modeled by commercial computational fluid dynamics (CFD) software (ANSYS 13). In particular, the solver used is Fluent. Given the computational tool that has been adopted, it was necessary to design a new virtual geometry for each folding angle. In its turn, a sufficiently fine mesh was created and customized for each case. In this sense, it was seen that the number of mesh elements in which the domains were discretized was directly proportional to the reduction in the

dx.doi.org/10.1021/ie302838m | Ind. Eng. Chem. Res. 2013, 52, 6916−6922

folding angle, resulting in a fine mesh with 811000 elements for the angle of 15.2°. This also augmented the times for convergence.

The simulation of the reactor consisted in the resolution of momentum and species mass balance equations. The energy balance was also solved but the medium was taken as isothermal, given that temperature has little effect on the catalyst photoactivity. The superficial reaction rate, which depends on the radiation flux, provides the link between the mass balance and the radiation balance.

In order to compute the radiation flux reaching the photocatalyst area (q_{inc}) and the LSRPA, a model was developed ad hoc. The radiation flux that reaches the reactor window was evaluated by means of a ray tracing method and a superficial emission model for the lamps. The air is taken as a nonparticipating medium. On the other hand, the walls of the triangular channels interchange radiation by means of absorption and reflection. These phenomena, evaluated by determination of optical properties, are used to compute the incident radiation on each surface. This modeling is achieved through the use and computation of local view factors, which are also called configuration factors.

The view factor for two infinitesimal surface elements, dA_1 and dA_2, is the fraction of energy exiting an isothermal, opaque, and diffuse surface 1 (by emission or reflection), that directly impinges on surface 2 (and is absorbed or reflected). View factors only depend on geometry and can be computed from well-known expressions.[21] The evaluation of the view factors was made by a numerical code. In the first term, the two photocatalytic surfaces of the channel were divided into small area elements; after the discretization, the view factors were computed for each element against each other by means of an integration procedure. Finally, the linear system resulting of the interaction of all the area elements was solved by a Gauss−Seidel method. More details regarding the theoretic and evaluation of view factor can be found elsewhere.[12] The incident radiation flux on each channel was then calculated for the different angles.

3.3. Results and Discussion. The lamps that were used for the experiments (Sylvania F15W BL350) have an input power of 15 W; their output power, within the wavelength range of 300−400 nm, was computed to be 4.16 W, according to the spectral emission provided by the manufacturer. Then, the electrical efficiency results in

$$\eta_{ele} = \frac{4.16\,W}{15\,W} = 0.277 \tag{6}$$

The number of lamps is five on each side and the lamps are not at the same distance from the reactor wall, in order to provide a nearly uniform incident radiation flux over the reactor window. For further details on the lamps arrangement, the reader is referred to a previous work.[9] The total computed radiation reaching each reactor window is 3.6 W. Thus, the outer geometrical incidence efficiency is

$$\eta_{inc}^{out} = \frac{3.6\,W}{5 \times 4.16\,W} = 0.173 \tag{7}$$

This specific value may be doubled if two reactor units are placed at the sides of a central radiation source with an equal number of lamps. Besides, η_{inc}^{out} could also be increased if the distance of the lamps to the reactor window is shortened.

Regarding the inner incidence efficiency (η_{inc}^{in}), a thorough analysis was performed to evaluate its dependence with the folding angle φ. As previously stated, a numerical ad hoc written script was executed for different folding angles based on the computation of view factors. In the first place, the evaluation of the incident flux was performed for different folding angles. The results, presented in Figure 2, correspond to

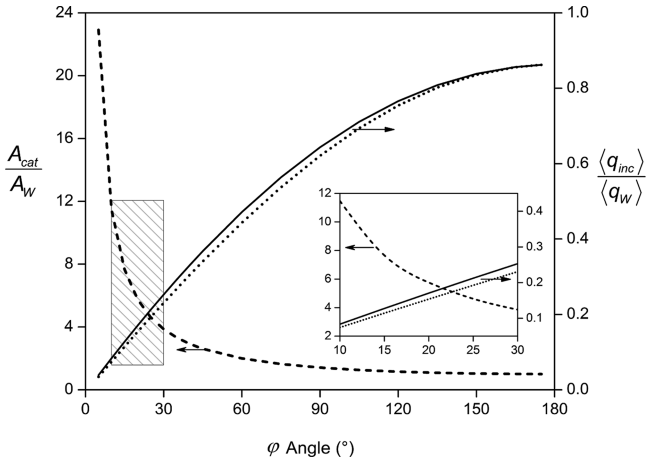

Figure 2. Relative incident radiation flux and catalytic area as a function of folding angle. Legend: (- - -) relative catalytic area per unit reactor window area, (—) relative incident radiation flux with reflective catalyst coating, and (···) relative incident radiation flux with no reflection (hypothetical case).

the cases with the experimentally determined spectral reflectance in a spectrophotometer Optronic OL Series 750 equipped with an integrating sphere OL 740−70 (continuous line) and a hypothetical case with no reflection at all (dotted line); a slight difference between both cases can be observed, with the largest values corresponding to the case of reflective catalyst layer. Figure 2 also includes a plot of the relative catalytic area per unit window area (dashed line); the curve shows an expected strong inverse relationship with the folding angle. The inset in Figure 2 is an enlargement of the shaded area, where the curves cross each other, indicating the possible optimum range for the folding angle φ.

The curves plotted in Figure 2 show an opposed behavior for two variables (A_{cat}/A_W and $\langle q_{inc}\rangle/\langle q_W\rangle$) which, if multiplied, determine the inner incidence efficiency in eq 2. In fact, given that η_{inc}^{in} is defined as the product of these two variables, the occurrence of a maximum might be supposed and then an optimal folding angle could be identified.

The influence of the folding angle on the inner incidence efficiency is depicted in Figure 3 for two cases: a reflecting catalyst surface and the hypothetical nonreflecting catalyst with the same spectral absorbing capacity. It can be seen that this parameter shows an optimum value at rather closed folding angles. Nevertheless, for the case with no reflection from the catalyst surface, the optimum is lower and the maximum presents a broader peak. For the real case (with reflection), the optimum value for η_{inc}^{in} is found at an angle of 20°. The fraction of absorbed radiation clearly enhances the capabilities of this corrugated wall configuration.

The curves in Figure 3 show results that are physically consistent: when the folding angle tends to zero, radiation can barely enter the reactor and η_{inc}^{in} falls drastically. In the opposite case, when the folding angle tends to 180°, the corrugated plate would be acting as a flat plate, and the distance between the two curves approaches zero because reflection is no longer

dx.doi.org/10.1021/ie302838m | Ind. Eng. Chem. Res. 2013, 52, 6916−6922

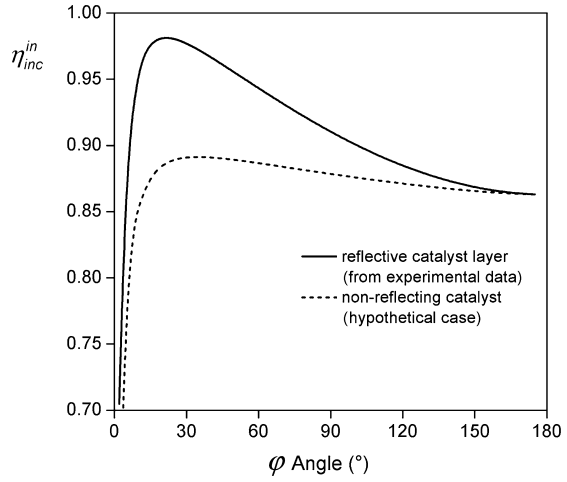

Figure 3. Inner incidence efficiency, as a function of folding angle.

important. Besides, for the most obtuse angles, the values of η_{inc}^{in} are very similar to the global view factor for two flat rectangles opposing one another,[22] which was found to be 0.87. The results for these two limiting cases indicate the consistency of the model.

The absorption capacity of the corrugated reactors for different folding angles was obtained prior to the reaction simulations. The results depicted in Figure 4 present the

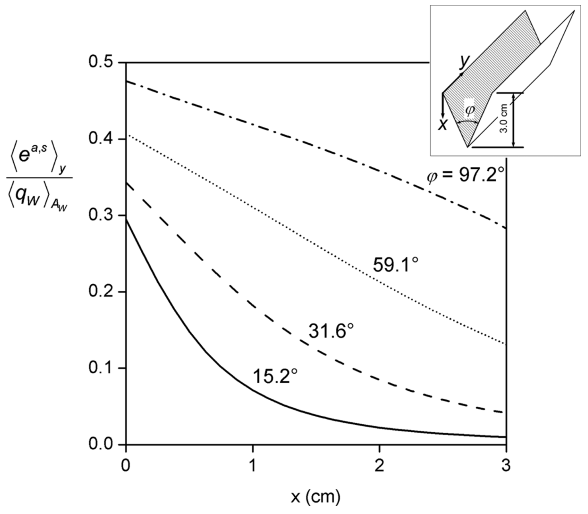

Figure 4. Relative *y*-averaged radiation absorption as a function of reactor depth for different folding angles.

relative *y*-averaged absorbed radiation as a function of reactor depth (x). The curves are parametric in the folding angle and indicate that the surface absorbs more radiation when the angle is more open. At this point, it is worth saying that, although the absorption efficiency (η_{abs}) is independent of the folding angle (from eq 3), there is a decrease in the relative absorption ($\langle e^{a,s}\rangle_y/\langle q_W\rangle_{A_W}$) toward smaller angles, because of the lower radiation penetration into each channel. The curves in Figure 4 suggest that the reactor should give better results when the folding angle is more open. Nevertheless, it may not be true when the relative catalytic area is taken into account.

The reaction efficiency η_{rxn} was evaluated through the CFD software. The radiation flux entering the reactor was computed externally by means of a numerical FORTRAN code, and its results were introduced by user-defined functions (UDF) into the FLUENT Solver; the code was based on the superficial emission model for the lamps and a ray tracing method.

In the FLUENT solver, the four folding angles were simulated; a new geometry was created for each one and the radiation fluxes accordingly established. The simulations included the resolution of momentum and species mass balance equations, subjected to the fixed operating variables: air flow rate, inlet pollutant concentration and radiation flux. The reaction kinetics was also introduced as UDF; the reaction rate expression is

$$r_F\left(\frac{\text{mol}}{\text{cm}^2\ \text{s}}\right) = -\frac{(1.34 \times 10^8)e^{a,s}C_F}{1.37 + (7.17 \times 10^9)C_F} \quad (8)$$

where the concentration of formaldehyde C_F is given in units of mol cm^{-3} and the parameter $e^{a,s}$ in given in units of einstein cm^{-2} s^{-1}. The kinetic expression and the parameter values were determined and presented in a previous work.[9]

The results of formaldehyde field concentrations for corrugated reactors with different folding angles are shown in Figure 5. The computed profiles show how the reactant is consumed at the catalytic walls, resulting in a maximum concentration at the center of the cross section of every channel. Also, there is a noticeable difference among the progress of the reaction, according to the folding angle.

The results of the modeling are summarized in Table 1. In addition to the reaction efficiency computed with the software output results, the inner incidence efficiency and the relative absorbed radiation are also included to enable comparison and analysis. The second column of Table 1 contains the absorbed energy relative to the entering radiation through the window; as can be seen, it increases when the folding angle becomes more open (obtuse), i.e., when the catalyst surface is almost normal to the radiation source. The third column of results shows the pollutant conversion at the outlet, computed by the expression $X = (C_{out} - C_{in})/C_{in}$, which presents an inverse but smooth dependence with the folding angle. On the other hand, the average superficial reaction rate (fourth column) increases almost 5-fold when opening the angle from 15.2° to 97.2°; this behavior may be explained by the strong linear dependence of the reaction rate with the absorbed radiation (eq 8). Finally, the fifth column presents the reaction efficiency, which is an indirect result derived from the previous columns; as can be seen, η_{rxn} has an almost constant value with a smooth trend to decrease when the folding angle is increased. This behavior can be interpreted as a result of the simultaneous increase in the relative absorbed energy (by a factor of 5) and the average superficial reaction rate (which is almost 5-fold increased).

The results presented in Table 1 indicate the presence of an optimum between the closest angles simulated, i.e., 15° and 30°. This is consistent with the maximum found for the inner incident efficiency (see Figure 3).

For illustrative purposes, the approach of efficiencies in series was applied to experimental data of a previously published work.[12] The corrugated reactor used there (where the elimination of formaldehyde was tested) had a very similar configuration to that described in Section 3. Consequently, with the exception of the reaction efficiency, all the other efficiencies are essentially the same. For instance, in an experimental run with an inlet concentration of 4.5 ppmv and the same radiation flux used here, the observed reaction efficiency was 8.4×10^{-4} (mol einstein^{-1}), which provides a

dx.doi.org/10.1021/ie302838m | Ind. Eng. Chem. Res. 2013, 52, 6916−6922

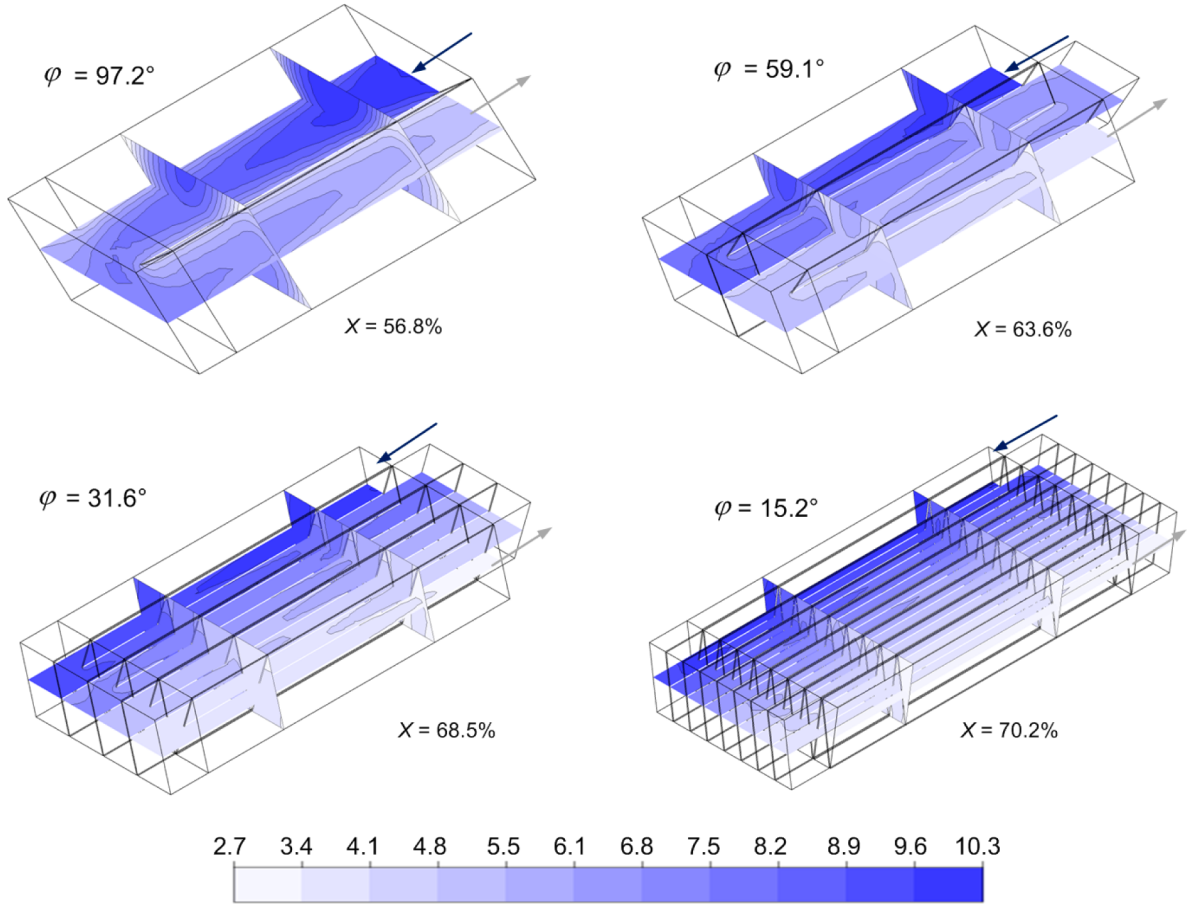

Figure 5. Formaldehyde concentration fields (in ppmv) and conversions at the outlet for different folding angles. C_F^{in} = 10.3 ppmv.

Table 1. Comparison of Reaction Parameters for Different Folding Angles

angle (°)	$\langle e^{a,s}\rangle/\langle q_W\rangle$	X (%)	$\langle R_{sup}\rangle \times 10^{11}$ (mol cm^{-2} s^{-1})	$\eta_{rxn} \times 10^3$ (mol einstein^{-1})	η_{inc}^{in}
15.2	0.078	70.2	1.04	9.24	0.978
31.6	0.155	68.5	2.09	9.29	0.976
59.1	0.271	63.6	3.50	8.93	0.944
97.2	0.395	56.8	4.74	8.28	0.903

difference of 6% when compared to the model result of 8.9 × 10^{-4} (mol einstein^{-1}). This represents a satisfactory validation of the computed results.

4. CONCLUSIONS

The concept of multiple efficiencies in series was developed and applied to the examination of the performance of photocatalytic wall reactors. The approach allowed the identification of critical parameters, which may be individually enhanced toward an optimal design of photoreactors.

An application of the multiple efficiencies in series was performed to a corrugated-wall, triangular-channel reactor. The new concept of inner incidence efficiency was introduced and its application proved to be useful for optimizing the photocatalytic wall reactor. In terms of this inner incidence efficiency, the main variable to optimize was the folding angle, given certain operating and geometric constraints. The calculation of outer geometrical and inner incidence efficiencies was performed by means of specifically written numerical codes; in contrast, the reaction efficiency was evaluated through FLUENT, a CFD software. Different geometries, corresponding to four folding angles, were studied and the conversion of pollutant was extracted. According to the values of the spectral reflectance of the catalyst layer, experimentally determined in a spectrophotometer equipped with an integrating sphere, the simulations showed an optimum folding angle between 15° and 30°.

AUTHOR INFORMATION

Corresponding Author

*Tel.: +54 0 342 457 5233. E-mail: rbrandi@santafe-conicet.gov.ar.

Notes

The authors declare no competing financial interest.

ACKNOWLEDGMENTS

The authors are grateful to Universidad Nacional del Litoral (UNL), Consejo Nacional de Investigaciones Científicas y Técnicas (CONICET), and Agencia Nacional de Promoción Científica y Tecnológica (ANPCyT) for the financial support.

NOMENCLATURE

A_{cat} = area for catalytic reaction (cm^2)
A_W = area of radiation entrance to the reactor (cm^2)
$e^{a,s}$ = local superficial rate of photon absorption (einstein cm^{-2} s^{-1})
Q_g = volumetric gas flow rate (cm^3 s^{-1})
q_W^{out} = radiation flux reaching the reactor window (einstein cm^{-2} s^{-1})

P_L = output power of the lamps (einstein s^{-1})
C_i = concentration (mol cm^{-3})
R_L = lamp radius (cm)
V = reactor volume (cm^3)
x,y,z = coordinate system

Greek Letters

λ = radiation wavelength (nm)
τ = spectral transmittance (dimensionless)
η_i = efficiency (dimensionless)
φ = folding angle (rad)

Special Symbols

$\langle\cdot\rangle$ = indicates an averaged property

Subscripts

abs = relative to radiation absorption
inc = indicates incident radiation
W = relative to reactor window; also refers to water

Superscripts

in = relative to inner reactor configuration
out = relative to outer reactor configuration

REFERENCES

(1) Jones, A. P. Indoor air quality and health. *Atmos. Environ.* **1999**, *33*, 4535−4564.
(2) Bruce, N.; Perez-Padilla, R.; Albalak, R. Indoor air pollution in developing countries: A major environmental and public health challenge. *B. World Health Org.* **2000**, *78*, 1078−1092.
(3) Wang, S.; Ang, H. M.; Tade, M. O. Volatile organic compounds in indoor environment and photocatalytic oxidation: State of the art. *Environ. Int.* **2007**, *33*, 694−705.
(4) Cassano, A. E.; Martin, C. A.; Brandi, R. J.; Alfano, O. M. Photoreactor analysis and design: Fundamentals and applications. *Ind. Eng. Chem. Res.* **1995**, *34*, 2155−2201.
(5) Raupp, G. B.; Alexiadis, A.; Hossain, M. M.; Changrani, R. First-principles modeling, scaling laws and design of structured photocatalytic oxidation reactors for air purification. *Catal. Today* **2001**, *69*, 41−49.
(6) Esterkin, C. R.; Negro, A. C.; Alfano, O. M.; Cassano, A. E. Air pollution remediation in a fixed bed photocatalytic reactor coated with TiO_2. *AIChE J.* **2005**, *51*, 2298−2310.
(7) Imoberdorf, G. E.; Cassano, A. E.; Irazoqui, H. A.; Alfano, O. M. Simulation of a multi-annular photocatalytic reactor for degradation of perchloroethylene in air: Parametric analysis of radiative energy efficiencies. *Chem. Eng. Sci.* **2007**, *62*, 1138−1154.
(8) Salvadó-Estivill, I.; Brucato, A.; Li Puma, G. Two-Dimensional Modeling of a Flat-Plate Photocatalytic Reactor for Oxidation of Indoor Air Pollutants. *Ind. Eng. Chem. Res.* **2007**, *46*, 7489−7496.
(9) Passalía, C.; Martínez Retamar, M. E.; Alfano, O. M.; Brandi, R. J. Photocatalytic Degradation of Formaldehyde in Gas Phase on TiO_2 Films: A Kinetic Study. *Int. J. Chem. React. Eng.* **2010**, 8.
(10) Zazueta, A. L. L.; Destaillats, H.; Li Puma, G. Radiation field modeling and optimization of a compact and modular multi-plate photocatalytic reactor (MPPR) for air/water purification by Monte Carlo method. *Chem. Eng. J.* **2013**, *217*, 475−485.
(11) Shang, H.; Zhang, Z.; Anderson, W. A. Nonuniform radiation modeling of a corrugated plate photocatalytic reactor. *AIChE J.* **2005**, *51*, 2024−2033.
(12) Passalía, C.; Alfano, O. M.; Brandi, R. J. Modeling and experimental verification of a corrugated plate photocatalytic reactor using computational fluid dynamics. *Ind. Eng. Chem. Res.* **2011**, *50*, 9077−9086.
(13) Ibrahim, H.; De Lasa, H. Novel photocatalytic reactor for the destruction of airborne pollutants reaction kinetics and quantum yields. *Ind. Eng. Chem. Res.* **1999**, 3211−3217.
(14) Serpone, N. Relative photonic efficiencies and quantum yields in heterogeneous photocatalysis. *J. Photochem. Photobiol. A* **1997**, *104*, 1−12.
(15) Singh, M.; Salvado-Estivill, I.; Li Puma, G. Radiation Field Optimization in Photocatalytic Monolith Reactors for Air Treatment. *AIChE J.* **2007**, *53*, 678−686.
(16) Bolton, J. R.; Bircher, K. G.; Tumas, W.; Tolman, C. A. Figures-of-merit for the technical development and application of advanced oxidation processes. *J. Adv. Oxid. Technol.* **1996**, *1*, 13−17.
(17) Hernandez, J. M. G.; Rosales, B. S.; De Lasa, H. The photochemical thermodynamic efficiency factor (PTEF) in photocatalytic reactors for air treatment. *Chem. Eng. J.* **2010**, *165*, 891−901.
(18) Mo, J.; Zhang, Y.; Yang, R. Novel insight into VOC removal performance of photocatalytic oxidation reactors. *Indoor Air* **2005**, *15*, 291−300.
(19) Cerdá, J.; Marchetti, J. L.; Cassano, A. E. Radiation efficiencies in elliptical photoreactors. *Lat. Am. J. Heat Mass Transfer* **1977**, *1*, 33−63.
(20) Ozisik, N. *Radiative Transfer and Interactions with Conduction and Convection*; Wiley: New York, 1973.
(21) Siegel, R.; Howell, J. *Thermal radiation heat transfer*; 4th ed.; Taylor & Francis: New York, 2002.
(22) Howell, J. R. *A Catalog of Radiation Heat Transfer Configuration Factors*. URL: http://www.me.utexas.edu/~Howell/sectionc/C-11.html, accessed Oct. 10, 2012.